Agglomeration and transport of drilling generated particles in directional oil wells

Ricardo Barros,[1] Panagiotis Giounanlis,[2] Susana Gomes,[3] Dan Lucas,[2,*] Orlaith Mannion,[1] Rachel Mulungye,[2] Brendan Murray,[2] Lennon Ó Náraigh,[2,†] and Timothy Simmons[4]

[1] *University of Limerick, Limerick, Ireland*

[2] *University College Dublin, Belfield, Dublin 4, Ireland*

[3] *Imperial College London, London SW7 2AZ, United Kingdom*

[4] *Herriott–Watt University, Riccarton, Currie EH14 4AS, United Kingdom*

(Dated: August 29, 2014)

EXECUTIVE SUMMARY

The work considered in this report was proposed by IRIS – International Research Institute of Stavanger – during the 102nd European Study Group with Industry, hosted by University College Dublin, Ireland, 30th June – 4th July 2014. The challenge presented by IRIS was to develop a better understanding of agglomeration and transport of cuttings generated during the drilling of an oil well.

There is a myriad of challenges involved in the mathematical modelling of this complex process. For this reason, two complementary approaches are combined in this report. First, we derive a one-dimensional fully-developed model based on the Phillips-type shear induced diffusive migration. We start by assuming a Newtonian nature of the suspending drilling mud, but an extension to account for a non-Newtonian rheology is proposed herein. Second, a direct numerical simulation approach is employed to predict settling rates of drilling cuts when the assumptions made in Part 1 break down and when complex geometries are taken into account.

* Principal author of the text in Part 2, with contributions from Brendan Murray

† Principal author of the text in Part 1, with contributions from Ricardo Barros

Email:

Ricardo Barros (ricardo.barros@ul.ie)

Panagiotis Giounanlis (panagiotis.giounanlis@ucdconnect.ie)

Susana Gomes (s.gomes12@imperial.ac.uk)

Dan Lucas (dan.lucas@ucd.ie)

Orlaith Mannion (13075934@studentmail.ul.ie)

Rachel Mulungye (rachel.mulungye@ucdconnect.ie)

Brendan Murray (brendan.murray@ucdconnect.ie)

Lennon Ó Náraigh (onaraigh@maths.ucd.ie)

PROBLEM STATEMENT AND MODELLING PHILOSOPHY

When drilling an oil well, rock cuttings are generated and must be transported to the surface for disposal. For this purpose, drilling fluid (or 'mud') is pumped down inside the drill pipe and exits at the drill bit. There, the drilling fluid combines with the rock cuttings whereupon both are transported through the annulus of the well back to the surface. The cuttings are then separated from the mud as required. This basic process is made complicated by a number of factors. First, the rheology of the drilling fluid is non-Newtonian. Although drilling fluid is normally oil-based or water-based, particles are added to give it a non-Newtonian (shear-thinning) rheology, so as to enhance the transport of the mixture of drilling fluid and cuttings to the surface. Secondly, an oilwell may have significant inclination ('directional wells'), meaning that the cuttings can 'settle' at the bottom of the annulus, forming a 'cuttings bed' potentially leading to clogging of the well. Finally, the drilling is a transient operation characterized by frequent start-ups and shut-downs: typically, the drilling is halted periodically to enable strands of drill pipe to be added as the well grows longer. Frequent shut-downs promote settling and therefore contribute to cuttings-bed formation. The fundamental problem addressed in this Report is to develop a physics-based understanding of the cuttings bed. From a practical aspect this is crucial, as poor control of cuttings may cause critical situations and a loss of the well.

In this work, two complementary approaches are taken. In the first approach ("Theoretical Modelling", Part 1), a continuum theory is formulated on the basis that a mixture of drilling fluid and cuttings can be treated in a fluid-mechanical framework. Existing methods concerning dense suspensions can then be applied (and improved as necessary) to predict settling rates as a function of input parameters. For small cutting sizes, such an approach is justified. However, for larger cutting sizes (e.g. rock cuttings comparable to the size of the annular region of the flow domain), such a continuum theory will inevitably break down. To understand the transport processes in this limit, direct numerical simulation is proposed (Part 2). Sample simulations using the freely available OpenFoam fluid solver are presented and future work to improve and refine the computational model is discussed.

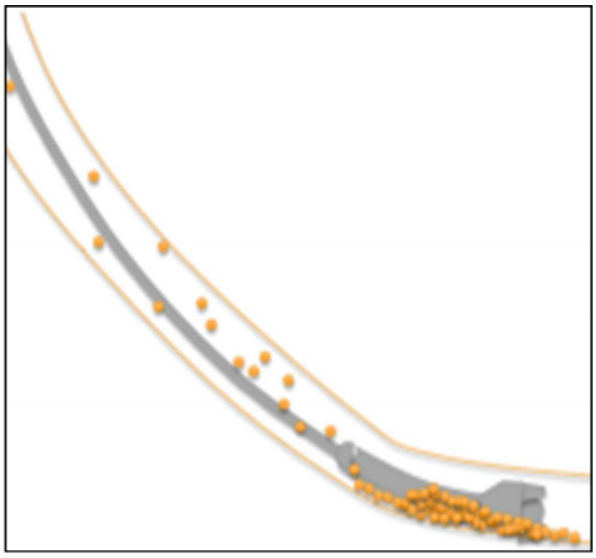

FIG. 1. Schematic picture of cuttings transport in a directional well

Part I
Theoretical Modelling

In this section we formulate a continuum theory for a dense suspension comprising a mixture of cuttings and drilling fluid. Mass and momentum conservation laws are written down for the mixture velocity and the volume fraction of the cuttings. Before doing this we examine the literature concerning dense suspensions and discuss the distinct but consistent model frameworks that can be used for these purposes.

I. LITERATURE REVIEW

At least two distinct approaches to modelling a suspension of dense particles in a (Newtonian) liquid exist in the literature. In the first approach, called the *suspension balance model*, the averaged dynamics of the suspended particles are described in a statistical-mechanics formalism. However, the model couples to the fluid mechanics of the problem in a natural way. This model was first proposed by Nott and Brady [37]. A review of the model (along with various refinements thereto) can be found in the work by Fang et al. [9], Morris and Brady [22]. The model involves mass and momentum equations for the particle phase (averaged over a test volume) and the mixture (again averaged over a test volume), leading to four evolutionary equations in the first instance. Both momentum equations involve particle-phase and mixture stress tensors respectively, and the particle momentum equation further involves a hydrodynamic drag force, meaning that three constitutive relations are required for closure. The closure is achieved by modelling the hydrodynamic drag force and various viscous terms. The particle-phase shear stress term is modelled by the introduction of an auxiliary variable (the particle-phase 'temperature'), leading to a set of five coupled evolution equations.

A simpler approach that makes predictions of comparable accuracy to the suspension-balance model is the *diffusive-flux model*, first introduced by Phillips et al. [40] but based partly on earlier work by Leighton and Acrivos [18] (see also the work by Schaflinger [43]). The idea here is to focus entirely on the mixture for the hydrodynamic model, leading to the basic equation

$$\rho(\phi)\left(\frac{\partial \boldsymbol{u}}{\partial t} + \boldsymbol{u}\cdot\nabla\boldsymbol{u}\right) = \nabla\cdot\boldsymbol{T} + \rho(\phi)\boldsymbol{g}, \tag{1}$$

together with the incompressibility condition $\nabla\cdot\boldsymbol{u} = 0$. Here, $\boldsymbol{u}(\boldsymbol{x}, t)$ is the Eulerian velocity of a parcel comprising a mixture of particles and suspending fluid. Thus, the density is given by

$$\rho(\phi) = \rho_{\mathrm{p}}\phi + \rho_{\mathrm{f}}(1-\phi), \tag{2}$$

where ϕ is the particle-phase volume fraction, ρ_{f} is the constant fluid density and ρ_{p} is the particle density, also constant. Finally, $\boldsymbol{g} = (0, 0, -g)$ is the acceleration due to gravity and $\boldsymbol{T}$ is the total mixture stress tensor. The evolution of the volume fraction ϕ is given by a flux-conservative equation,

$$\frac{\partial\phi}{\partial t} = \nabla\cdot\boldsymbol{J}_{\phi}, \tag{3}$$

where the particle flux $\boldsymbol{J}_{\phi}$ is modelled according to the collision dynamics of the particles. The collective particle dynamics are classified according to the following effects:

- *Shear-induced migration:* In a dense suspension, particles that are transported by a shear flow will collide. The collision rate is proportional to $\phi\dot{\gamma}$, where $\dot{\gamma}$ is the local shear rate. Particles will move from regions where the collision rate is high to a nearby region where the collision rate is lower, meaning that there is a shear-induced contribution $\boldsymbol{J}_\mathrm{c}$ to the total flux, with $\boldsymbol{J}_\mathrm{c} \propto -\nabla(\phi\dot{\gamma})$. Phillips et al. [40] give the shear-induced flux as

$$\boldsymbol{J}_\mathrm{c} = -D_\mathrm{c}\phi a^2 \nabla\left(\phi\dot{\gamma}\right), \tag{4}$$

  where D_c is a dimensionless constant and a is the particle radius (a monodisperse suspension of identical spherical particles is assumed).

- *Viscous migration:* Again in a dense suspension, and under collisions, particles will move into regions of lower viscosity, from regions of higher viscosity. Phillips et al. [40] note that the viscous contribution to the total flux is proportional to the ratio between the viscosity gradient (giving the direction of migration) and the local viscosity, giving a total contribution

$$\boldsymbol{J}_\mathrm{v} = -D_\mathrm{v}\phi a^2 \phi\dot{\gamma}\left(\frac{\nabla\mu}{\mu}\right), \tag{5}$$

  where D_v is another dimensionless constant.

- *Settling:* For particles whose density is greater than that of the suspending fluid, settling will occur, leading to a gravitational flux. For Stokes flow, this can be modelled as

$$\boldsymbol{J}_\mathrm{g} = -\frac{2a^2(\rho_\mathrm{p}-\rho_\mathrm{f})f(\phi)}{9\mu_\mathrm{f}}\boldsymbol{g}, \tag{6}$$

  where μ_f is the (constant) dynamic viscosity of the suspending fluid, and $f(\phi)$ is the so-called 'hindrance function', introduced here because the collective settling flux in a suspension differs from the corresponding single-particle expression because neighbouring particles 'hinder' a given particle's descent through the medium. Using the same reasoning, walls also hinder settling, and exact expressions for single-particle settling in the neighbourhood of a wall are known [11]; these effects may be parametrized through a modification of Equation (6):

$$\boldsymbol{J}_\mathrm{g} = -\frac{2a^2(\rho_\mathrm{p}-\rho_\mathrm{f})f(\phi)}{9\mu_\mathrm{f}}\boldsymbol{g}\,\omega(z). \tag{7}$$

  Expressions for $\omega(z)$ can be found in the literature. Here we use

$$\omega(z) = A(z/a)^2\sqrt{1+A^2(z/a)^4},$$

  with $A = 1/18$, *cf.* Reference [23], so that $\omega(z) \to 0$ as $z \to 0$ and $\omega \approx 1$ away from $z = 0$. Also, numerous (and very similar) forms exist for the hindrance function (e.g. Reference [47]); here we use $f(\phi) = (1-\phi)\mu_\mathrm{f}/\mu(\phi)$, where $\mu(\phi)$ is the effective viscosity of the suspension. For dense suspensions, the Krieger–Dougherty relation is appropriate here, giving the effective suspension viscosity as

$$\mu(\phi) = \mu_\mathrm{f}\left(1-\frac{\phi}{\phi_\mathrm{m}}\right)^{-\xi}, \tag{8}$$

  where ξ is a positive constant and $\phi_\mathrm{m} > 0$ is the maximum volume fraction achievable by the spherical particles.

- *Brownian flux:* The considered model is isothermal and a specific temperature $T > 0$ is assumed. At finite temperatures, the particles will experience thermal fluctuations, giving rise to a purely Brownian flux term $\boldsymbol{J}_{\mathrm{d}} = -D\nabla\phi$, where D is the diffusivity. The importance of the diffusivity is estimated through the particle Péclet number, $Pe = \dot{\gamma}a^2/D$. For the present applications, this is typically a large number [40], meaning that the Brownian contribution to the total flux can be ignored.

- *Wall effects not included here:* For neutrally buoyant particles, wall effects may also be important. Indeed, numerical simulations [50] and experiments [19] in pressure-driven flow in Hele–Shaw geometries show 'depletion layers' in near-wall regions that are not explained by the factors previously listed. The existence of such depletion layers is not really surprising: for a particle to enter a particular region, it must extrude an equivalent volume of fluid from the same region. This process will be different depending on whether one is in a near-wall or a bulk region: close to the wall, the process will be relatively more difficult to achieve, since the fluid must be expelled from a small gap where the no-slip condition on the fluid velocity is important, leading to a very large localized shear stress.

  A modelling approach that may be appropriate here is to include a flux term proportional to an effective short-range potential that parametrizes the "effective" repulsion experienced by the particles int he near-wall region. Such an approach already exists in the complex of suspension modelling for red blood cells in blood vessels [10], albeit that there the repulsive interaction term is a physical one, due to Van der Waals forces between the wall and the cells.

The modelling approach taken in this work is based on the diffusive flux description, as opposed to the suspension balance picture. The reasons for this are twofold: the diffusive flux framework is both conceptually and analytically straightforward, and involves only a handful of parameters, all of which can be estimated from benchmark cases. Although it has shortcomings [9], it produces acceptable results for flow profiles and volume profiles in pressure-driven channel and pipe flows, as well as in rotating shear flow [40]. We emphasize also that the foregoing discussions are based on the assumption that the suspending fluid has a Newtonian rheology. It will be discussed in §II B how this assumption can be relaxed. In order to do this fully consistently, the closure relation (6) for the gravitational flux should also be modified in this context. This is particularly important for flows with a finite yield stress, wherein particles do not begin to settle unless a critical buoyancy is attained.

II. THE MATHEMATICAL MODEL

Without making too many leaps into abstraction, the physical domain of the problem described schematically in Figure 1 is given as an annular region between two non-concentric cylinders, each of the same finite length. The two cylinders are inclined relative to the direction of gravity, but not necessarily by the same amount. Also, the inner cylinder rotates at a fixed rate, mimicking the effect of the rotating drill. However, this complex geometry is best addressed through direct numerical simulation (i.e. Part 2 of this Report), meaning that a simplified scenario is more appropriate for theoretical modelling. The idea is that fundamental understanding of the physics of cuttings transport can be obtained from simple models (both in steady state and transient modes), which can then be compared

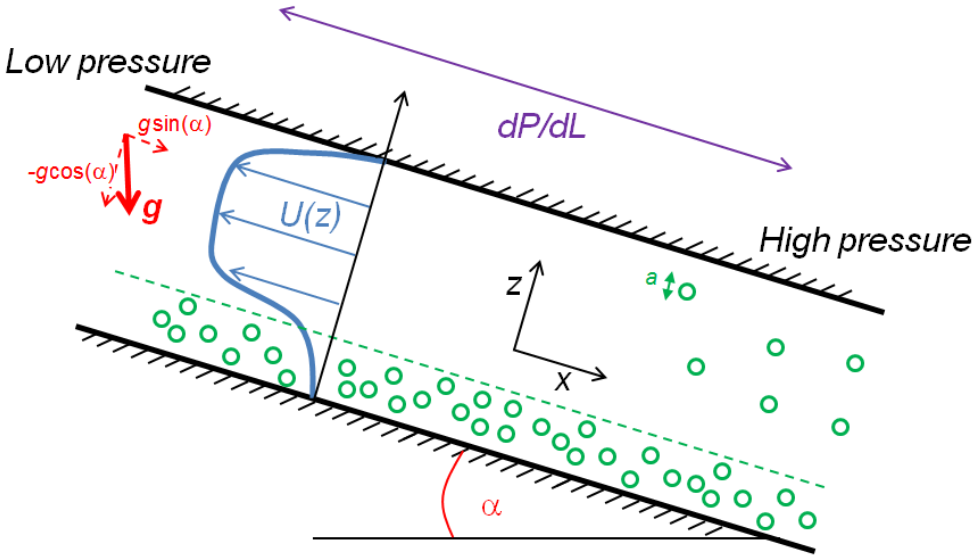

FIG. 2. Schematic description of reduced model

to direct numerical simulation model thereby accounting for the effects of geometry and rotation and ultimately enabling a comparison with experiment.

Therefore, we focus on cuttings transport in a cylindrical region and also more intensively on cuttings transport in a two-dimensional channel (Figure 2), with the understanding that the latter gives flow profiles and volume-fraction profiles that are indicative of the same profiles at the centreline of the cylinder. The main deliverable of this Report is therefore a mathematical model of a dense suspension under shear flow, valid in a channel flow. Again, the reason for focusing on this case is the need to make rapid analytical progress; also, the same simplicity will enable us to extend the channel-flow model and describe a tool that is highly appropriate for addressing the transient aspect of the stated problem.

A. Fully developed flow

We start by assuming that the total mixture stress tensor by $\boldsymbol{T} = -p\boldsymbol{I} + \boldsymbol{\sigma}$, in which p is the pressure, $\boldsymbol{\sigma} = 2\mu(\phi)\dot{\gamma}$, and where $\dot{\gamma} = (1/2)[\nabla\boldsymbol{u} + (\nabla\boldsymbol{u})^{\mathrm{T}}]$ is the (symmetric) rate-of-strain tensor. The particle flux $\boldsymbol{J}_\phi$ is modelled as $\boldsymbol{J}_\phi = \boldsymbol{J}_c + \boldsymbol{J}_v + \boldsymbol{J}_g$. Moreover, as already mentioned, we will be focusing on the flow at the centreline of the cylinder as in Figure 2.

If a fully developed flow is achieved, meaning that we are in a regime well downstream of the drill bit, such that equilibrium profiles for the mixture velocity and particle volume fraction are maintained, we should look for steady-state solutions with $\boldsymbol{u} = (U(z), 0, 0)$ and where a pressure gradient $dP/dL > 0$ is applied along the channel. We are justified in considering this regime in the first instance, since it provides an important base state in order to validate any transient flow calculations. Also, flow-pattern maps can be obtained that give the flow rate of the fluid and particle phases as a function of the problem parameters.

In this scenario, the relevant diffusive-flux equations read

$$\frac{\mathrm{d}\sigma}{\mathrm{d}z} = \frac{dP}{dL} - \rho(\phi) g \sin\alpha, \tag{9a}$$

$$0 = J_\mathrm{c} + J_\mathrm{v} + J_\mathrm{g}, \tag{9b}$$

where $\sigma = \mu(\phi)\dot{\gamma}$ is the shear stress of the mixture, and $\dot{\gamma} = dU/dz$ is the rate of strain. Here, the suspending fluid is assumed to be Newtonian; the effects of a non-Newtonian rheology in the suspending fluid are discussed at the end of this section. We nondimensionalize the equations of motion based on the channel height H and the characteristic velocity V, where

$$V = \frac{H^2}{\mu_\mathrm{f}} \frac{dP}{dL},$$

thereby introducing dimensionless variables $\tilde{z} = z/H$, $\tilde{U} = U/V$, $\widetilde{\dot{\gamma}} = \dot{\gamma}(H/V)$ and $\tilde{\sigma} = \sigma/\sigma_0$, with $\sigma_0 = \mu_\mathrm{f} V/H$. Also, all densities are scaled relative to the density ρ_f of the suspending fluid. Based on these scaling rules, and based on the closure relations for the fluxes described in Section I, the following non-dimensional equations of motion are obtained:

$$\frac{\mathrm{d}\tilde{\sigma}}{\mathrm{d}\tilde{z}} = 1 - \tilde{\rho}(\phi) \mathrm{Re}\,\mathrm{Fr}^2 \sin\alpha, \tag{10a}$$

$$0 = D_\mathrm{c}\epsilon^2\phi \frac{\mathrm{d}}{\mathrm{d}\tilde{z}}\left(\widetilde{\dot{\gamma}}\phi\right) + D_\mathrm{v}\epsilon^2\phi\widetilde{\dot{\gamma}}\frac{1}{\mu}\frac{\mathrm{d}\mu}{\mathrm{d}\tilde{z}} + \frac{2\epsilon^2(r-1)\phi(1-\phi)}{9\tilde{\mu}(\phi)}\mathrm{Re}\,\mathrm{Fr}^2\cos\alpha\,\omega(\tilde{z}), \tag{10b}$$

where $r = \rho_\mathrm{p}/\rho_\mathrm{f}$, $\tilde{\rho} = r\phi + (1-\phi)$, $\tilde{\mu}(\phi) = [1 - (\phi/\phi_\mathrm{m})]^{-\xi}$, $\epsilon = a/H$, and where

$$\mathrm{Re} = \frac{VH\rho_\mathrm{f}}{\mu_\mathrm{f}}, \qquad \mathrm{Fr}^2 = \frac{gH}{V^2}.$$

Following standard practice, the ornamentation over the dimensionless variables is now dropped. We next rewrite Equation (10b) in terms of σ, removing all instances of $\dot{\gamma}$ as follows:

$$D_\mathrm{c}\phi\frac{\mathrm{d}}{\mathrm{d}z}\left(\frac{\sigma}{\mu}\phi\right) + D_\mathrm{v}\phi\frac{\sigma}{\mu^2}\frac{\mathrm{d}\mu}{\mathrm{d}z} + \frac{2(r-1)\phi(1-\phi)}{9\mu(\phi)}\mathrm{Re}\,\mathrm{Fr}^2\cos\alpha\,\omega(z) = 0. \tag{11}$$

A simple rearrangement of terms leads to

$$\frac{\mathrm{d}\phi}{\mathrm{d}z} = \frac{-\phi\frac{\mathrm{d}\sigma}{\mathrm{d}z} + \frac{2}{9D_\mathrm{c}}\mathrm{Re}\,\mathrm{Fr}^2(r-1)(1-\phi)\cos\alpha\,\omega(z)}{\sigma\left[1 + 2\left(\frac{D_\mathrm{v}-D_\mathrm{c}}{D_\mathrm{c}}\right)\frac{\phi}{\phi_\mathrm{m}-\phi}\right]} \tag{12}$$

In practice, it is ill-advised to solve this equation because of the singularity at places where the shear stress vanishes (corresponding to the centreline in single-phase Poiseuille flow). This could be fixed by letting the collision rate go to zero when the shear rate vanishes, however this is unphysical. Another drawback of the model is that there is no influence of particle size on the solutions. For these reasons (and the main innovation of this section), we consider instead the shear stress averaged over a single spherical particle,

$$\hat{\sigma} = \sqrt{\sigma^2 + \epsilon^2\left(\frac{\mathrm{d}\sigma}{\mathrm{d}z}\right)^2}. \tag{13}$$

This can be regarded as a non-local improvement of the basic Phillips model; details of the averaging procedure are given in Appendix A. The expression for $\hat{\sigma}$ has the advantage of being manifestly positive, which is a requirement for any term proportional to the collision rate. The regularized version of Equation (12) now reads

$$\frac{\mathrm{d}\phi}{\mathrm{d}z} = \frac{-\phi\frac{\sigma}{\hat{\sigma}}\frac{\mathrm{d}\sigma}{\mathrm{d}z} + \frac{2}{9D_\mathrm{c}}\mathrm{Re}\,\mathrm{Fr}^2(r-1)(1-\phi)\cos\alpha\,\omega(z)}{\hat{\sigma}\left[1+2\left(\frac{D_\mathrm{v}-D_\mathrm{c}}{D_\mathrm{c}}\right)\frac{\phi}{\phi_\mathrm{m}-\phi} + \frac{\epsilon^2}{\hat{\sigma}^2}\frac{\mathrm{d}\sigma}{\mathrm{d}z}\mathrm{Re}\,\mathrm{Fr}^2(r-1)\sin\alpha\right]} \tag{14}$$

The equations to be solved are now in closed form and are gathered together here as follows:

$$\frac{dU}{dz} = \frac{\sigma}{\mu}, \tag{15a}$$

$$\frac{\mathrm{d}\sigma}{\mathrm{d}z} = 1 - \mathrm{Re}\,\mathrm{Fr}^2\left[r\phi + (1-\phi)\right]\sin\alpha, \tag{15b}$$

$$\frac{\mathrm{d}\phi}{\mathrm{d}z} = \frac{-\phi\frac{\sigma}{\hat{\sigma}}\frac{\mathrm{d}\sigma}{\mathrm{d}z} + \frac{2}{9D_\mathrm{c}}\mathrm{Re}\,\mathrm{Fr}^2(r-1)(1-\phi)\cos\alpha\,\omega(z)}{\hat{\sigma}\left[1+2\left(\frac{D_\mathrm{v}-D_\mathrm{c}}{D_\mathrm{c}}\right)\frac{\phi}{\phi_\mathrm{m}-\phi} + \frac{\epsilon^2}{\hat{\sigma}^2}\frac{\mathrm{d}\sigma}{\mathrm{d}z}\mathrm{Re}\,\mathrm{Fr}^2(r-1)\sin\alpha\right]}, \tag{15c}$$

together with the auxiliary condition (13). Also, we set $\mathrm{d}\phi/\mathrm{d}z = 0$ whenever $\phi = 0$ or $\phi = \phi_\mathrm{m}$. Equation (15) is therefore a two-point boundary value problem involving three first-order ordinary differential equations. Two boundary conditions are obvious: $U(0) = U(1) = 0$. In practice, the third boundary condition is prescribed as $\phi(0) = \phi_1$, and ϕ_1 is adjusted until the corresponding specified bulk cuttings volume fraction Φ is obtained, where

$$\Phi = \int_0^1 \phi(z)\,\mathrm{d}z. \tag{16}$$

The model ordinary differential equations (ODEs) (15) are solved in Matlab using a shooting method. Boundary conditions at $(U(0) = 0, \sigma(0) = \sigma_1, \phi(0) = \phi_1)$ are supplied and the parameter σ_1 is adjusted using a rootfinding procedure until the no-slip condition at $z = 1$ is also satisfied. The numerical method 'ode15s' is invoked in Matlab to handle the stiffness of the problem associated with the quantity $\hat{\sigma}$. The parameter space is multidimensional, and involves the five independent parameters $(\mathrm{Re}\,\mathrm{Fr}^2, r, \epsilon, \alpha, \Phi)$, with $D_\mathrm{c} = 0.43$, $D_\mathrm{v} = 0.65$, $\xi = 2$, $\phi_\mathrm{m} = 0.68$ set by theory. Also, the functional form for $\omega(z)$ is taken directly from Reference [23]. In the present context we have set $r = 2$, $\epsilon = 0.01$, and $\alpha = \pi/12$ and focus for the remainder of this section on the parameter subspace $(\mathrm{Re}\,\mathrm{Fr}^2, \Phi)$. Sample results are shown in Figure 3 for the case $\Phi = 0.35$ and various values of $\mathrm{Re}\,\mathrm{Fr}^2$. Here, in panel (a), the effect of gravity is small compared to the applied pressure gradient, and the mixture flows up the channel. The volume-fraction profile and the mixture flow profile are similar to those observed in pure pressure-driven channel flows, and the system is 'well mixed', in the sense that a nonzero volume fraction extends from the bottom wall to the top wall, with a maximum distribution of particles close to the channel centreline, corresponding to shear-induced migration. Upon increasing the gravity effect compared to the pressure effect (panel (b)), the system ceases to be well mixed, the particles settle, and a bed forms. The fluid velocity is correspondingly reduced to near-zero values in the bed, but the net flow of matter is still in the negative x-direction. Upon increasing the gravity effect further, complete flow reversal happens (panel (c)). These results also suggest the possibility of a near-stationary cuttings bed for suitable values of Φ and $\mathrm{Re}\,\mathrm{Fr}^2$. A sample of such a result is shown in Figure 4.

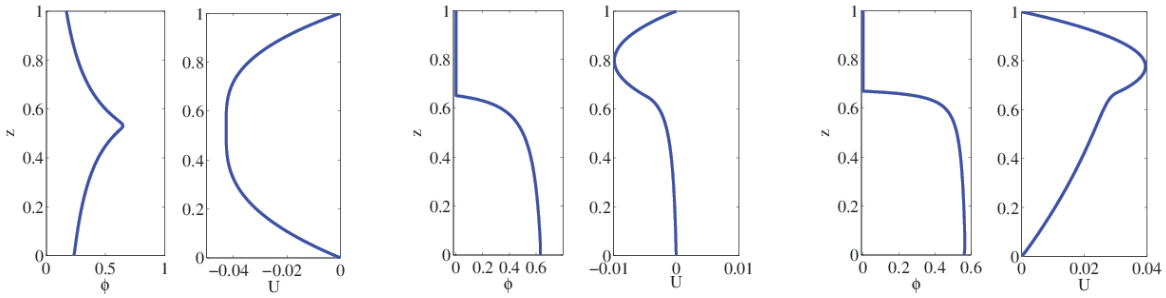

(a) $\mathrm{Re}\,\mathrm{Fr}^2 = 0.1$ (b) $\mathrm{Re}\,\mathrm{Fr}^2 = 2$ (c) $\mathrm{Re}\,\mathrm{Fr}^2 = 10$

FIG. 3. Sample profiles for $\Phi = 0.35$ and various values of $\mathrm{Re}\,\mathrm{Fr}^2$, corresponding to (a) weak gravity effect, (b) gravity effect finely balanced compared to pressure effect and (c) strong gravity effect. Increasing the gravity effect leads to flow reversal, corresponding to a change in the direction of the flow profile in (c). The values for the physical parameters r, ϵ, and α will be fixed throughout the text as $r = 2$, $\epsilon = 0.01$, and $\alpha = \pi/12$.

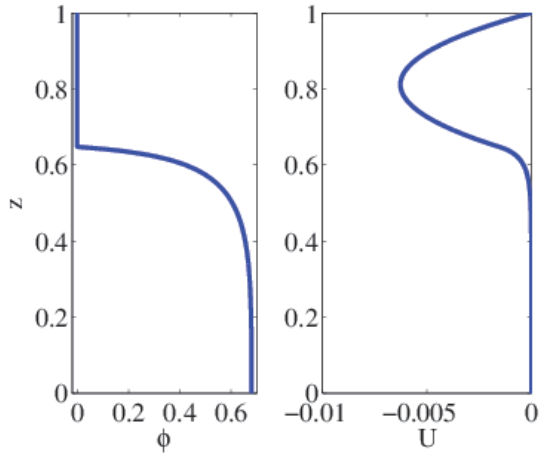

FIG. 4. Stationary cuttings bed with clear layer of drilling fluid transported upward ($\Phi = 0.4, \mathrm{Re}\,\mathrm{Fr}^2 = 2.5$).

To understand these trends in a more systematic way, contour plots of the mixture volumetric flow rate and the particle volumetric flow rate were obtained. These quantities are given by the respective equations

$$Q_{\text{mixture}} = \int_0^1 U(z)\,\mathrm{d}z, \qquad Q_{\text{particles}} = \int_0^1 \phi(z)U(z)\,\mathrm{d}z; \tag{17}$$

the fluid volumetric flow rate is obtained as $Q_{\text{fluid}} = Q_{\text{mixture}} - Q_{\text{particles}}$. The corresponding plots are shown in Figure 5. In both panels, there is a blank region in parameter space corresponding to large particle volume fractions Φ and intermediate values of $\mathrm{Re}\,\mathrm{Fr}^2$. In this region, no solution to the ODE system (15) exists. Physically, this region would correspond to a very high density of particles in a slow-moving or even stationary bed which is unsustainable as an equilibrium solution, and would correspond to a 'clogging scenario' in a real well, wherein the cuttings overwhelm the flow and lead to a breakdown in operations. In the same panel there is a critical curve $((\mathrm{Re}\,\mathrm{Fr}^2)_c, \Phi_c)$ (marked in a solid black line) wherein flow

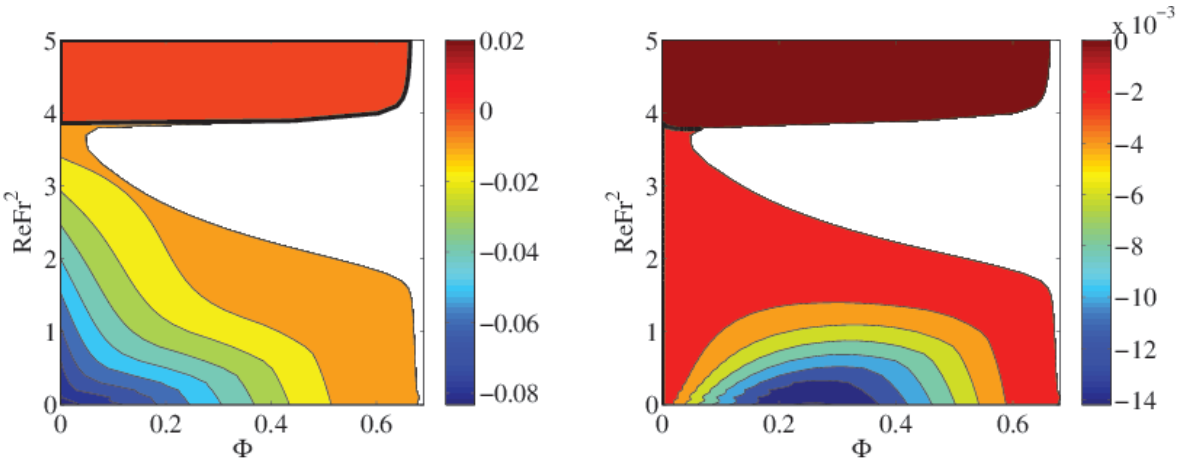

(a) Q_{mixture} (b) $Q_{\text{particles}}$

FIG. 5. (a) Mixture flowrate as a function of $(\Phi, \mathrm{Re}\,\mathrm{Fr}^2)$ showing flow reversal line $Q_{\text{mixture}} = 0$ at large values of $\mathrm{Re}\,\mathrm{Fr}^2$; (b) Particle flowrate, showing reveral of particle flux at $Q_{\text{particles}} = 0$.

reversal occurs and the mixture is transported down the length of the channel (as opposed to in the desired direction which is upwards). Mathematically, the condition for the onset of flow reversal is $\mathrm{d}\sigma/\mathrm{d}z = 0$ at $z = 0$, corresponding to $-1 + (r\phi_1 + (1 - \phi_1))\mathrm{Re}\,\mathrm{Fr}^2 \sin\alpha = 0$, hence

$$\phi_{1\mathrm{c}} = \frac{1 - \mathrm{Re}\,\mathrm{Fr}^2 \sin\alpha}{(r-1)\mathrm{Re}\,\mathrm{Fr}^2 \sin\alpha}. \tag{18}$$

The precise critical curve for the onset of flow reversal can therefore be obtained by solving Equation (15) as an initial value problem with $\sigma(0) = 0$, $\phi_1 = \phi_{1\mathrm{c}}$, for a range of values of $\mathrm{Re}\,\mathrm{Fr}^2$, which then enables one to generate 'operating envelope' $\Phi = \Phi(\mathrm{Re}\,\mathrm{Fr}^2)$ whose boundary gives the condition for flow reversal to occur.

B. Non-Newtonian rheology for the suspending fluid – outline

So far we have considered only the case wherein the drilling fluid possesses Newtonian rheology. In practice, this is not the case, as the drilling fluid is deliberately constituted so as to be highly shear-thinning, so as to enhance the 'cleaning' of the oil well. Also, the drilling fluid is thought to have a yield stress [15]. Indeed, the Herschel–Bulkley rheological model can be fitted to a class of standard drilling muds [15]. We outline the main changes required to the model in order to take account of the non-Newtonian rheology of the drilling fluid. Crucially, constitutive modelling of three quantities is required to close the non-Newtonian version of Equation (15):

1. A model for the settling viscosity in a Herschel–Bulkley fluid. Thus, equation (6) must be replaced by

$$\boldsymbol{J}_{\mathrm{g}} = -\phi M_{NN}(\phi, z)\mathrm{Fr}^2(\sin\alpha, 0, -\cos\alpha), \tag{19}$$

where the mobility function $M_{NN}(\phi, z)$ is to be determined, and where we work with a nondimensional system of equations.

2. A model for how the rheology of the non-Newtonian drilling mud is modified in the presence of particles. Not only is the rheology of the pure drilling fluid required, but also the rheology of the mixture of cuttings and drilling fluid must be determined. Thus, a constitutive relation of the (nondimensional) form

$$\mu(\phi) = k(\phi)\|\dot{\gamma}\|^{n(\phi)-1} + \frac{Bn(\phi)}{\|\dot{\gamma}\|} \tag{20}$$

is required, wherein $(k(0), n(0), Bn(0))$ correspond to a reversion to the rheological properties of the pure drilling fluid, i.e. $\phi = 0$. Here, $\|\dot{\gamma}\| = \sqrt{2\dot{\gamma}_{ij}\dot{\gamma}^{ij}}$ is the second invariant of the shear-rate tensor, where $\dot{\gamma} = (1/2)\left(\nabla\boldsymbol{u} + \nabla\boldsymbol{u}^T\right)$. Also, $k(\phi)$ is the non-dimensional consistency, $n(\phi)$ is the power and $Bn(\phi) = [\text{Yield stress}]/\sigma_0$ is the non-dimensional Bingham number. These considerations lead to a constitutive relation for the viscous component of the suspension stress tensor, $\boldsymbol{\tau} = 2\mu(\phi)\dot{\gamma}$.

Once these relations are supplied, the ODE system (15) can be reformulated as follows:

$$\frac{\mathrm{d}U}{\mathrm{d}z} = \begin{cases} \mathrm{sign}(\sigma)\frac{||\sigma|-Bn(\phi)|^{1/n(\phi)}}{k(\phi)}, & |\sigma| > Bn(\phi), \\ 0, & \text{otherwise}, \end{cases} \tag{21a}$$

$$\frac{\mathrm{d}\sigma}{\mathrm{d}z} = 1 - \mathrm{Re}\,\mathrm{Fr}^2\left[r\phi + (1-\phi)\right]\sin\alpha, \tag{21b}$$

$$\frac{\mathrm{d}\phi}{\mathrm{d}z} = \begin{cases} 0, & \text{if } \phi = 0, \text{ or } \phi = \phi_\mathrm{m}, \\ \frac{-\phi\frac{\sigma}{\hat{\sigma}}\frac{\mathrm{d}\sigma}{\mathrm{d}z} + \frac{1}{D_\mathrm{c}}Fr^2 M_{NN}(\phi,z)\cos\alpha}{\hat{\sigma}\left[1+2\left(\frac{D_\mathrm{v}-D_\mathrm{c}}{D_\mathrm{c}}\right)\frac{\phi}{\phi_\mathrm{m}-\phi} + \frac{\epsilon^2}{\hat{\sigma}^2}\frac{\mathrm{d}\sigma}{\mathrm{d}z}\mathrm{Re}\,\mathrm{Fr}^2(r-1)\sin\alpha\right]}, & \text{otherwise}. \end{cases} \tag{21c}$$

III. TRANSIENT OPERATION WITH TPLS - OUTLINE

Beyond the steady-state scenarios discussed in Section II, it is of interest to know how the suspension behaves under transient operation, without necessarily resorting to full-scale direct numerical simulations. The aim of the present section is therefore to discuss a simulation model capable of real-time prediction, using again the drift-diffusion model as a basis. For this purpose, we outline how an existing massively parallel open-source two-phase solver (TPLS) can be adapted for the simulation of dense suspensions.

TPLS (Two-Phase Level Set) is a Computational Fluid Dynamics code developed by the present author and Prashant Valluri of the University of Edinburgh's School of Engineering. It simulates the interface between two fluid phases by solving the two-phase Navier-Stokes equations with levelset interface capturing technology (e.g. Figure 6). Even for scenarios where the bulk flow is laminar, the interfacial structures can become quite complicated, and high-resolution simulation in three dimensions are required. These simulations can only be performed in a realistic timeframe on supercomputers. Thus, TPLS is fully parallelized for execution on machines with thousands of cores. A 2D MPI process decomposition coupled with a hybrid OpenMP parallelisation scheme allows scaling to 1000s of CPU cores. The code has been rigorously validated with respect to Orr-Sommerfeld, Orr-Sommerfeld-Squire, and Stuart-Landau semi-analytical theories, for a wide range of Reynolds numbers, viscosity ratios, density ratios, capillary numbers, etc., as described in Reference [45]. The code can be configured in co-current, countercurrent, horizontal, and vertical cases, with inlet/outlet

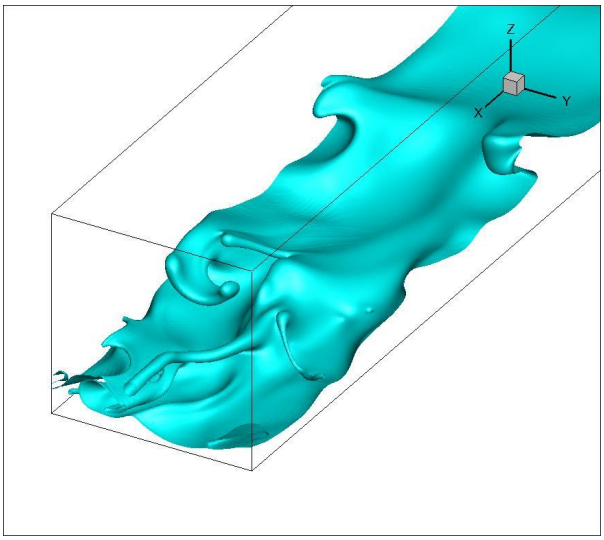

FIG. 6. Sample result from TPLS showing fine interfacial resolution. Note that the flow configuration in the figure is for illustration only and corresponds to a different physical regime to the one described in the present report. Specifically, in the figure, it is a two-phase Newtonian cocurrent flow with matched densities but a viscosity contrast across the (immiscible) interface. The mismatch in viscosities drives an instability which precipitates the formation of the complicated interfacial structures shown in the figure. See Reference [45].

boundary conditions or periodic boundary conditions. Currently the code is restricted to channel geometries in both two and three dimensions.

The basic (dimensional) equations to be solved are

$$\rho(\phi)\left(\frac{\partial \boldsymbol{u}}{\partial t}+\boldsymbol{u}\cdot\nabla\boldsymbol{u}\right)=-\nabla p+\nabla\cdot\left[\mu\left(\nabla\boldsymbol{u}+\nabla\boldsymbol{u}^{T}\right)\right]+\Sigma\delta_{\epsilon}(\phi)\hat{\boldsymbol{n}}\nabla\cdot\hat{\boldsymbol{n}}+\rho(\phi)\boldsymbol{g}, \tag{22a}$$

$$\nabla\cdot\boldsymbol{u}=0, \tag{22b}$$

$$\hat{\boldsymbol{n}}=\frac{\nabla\phi}{|\nabla\phi|}, \qquad \frac{\partial\phi}{\partial t}+\boldsymbol{u}\cdot\nabla\phi=0. \tag{22c}$$

Here, $\phi(\boldsymbol{x},t)$ is the levelset function indicating in which phase the point $\boldsymbol{x}$ lies ($\phi<0$ in the bottom layer, $\phi>0$ in the top layer). The (possibly multivalued) interface $\eta(\boldsymbol{x},t)$ is therefore the zero level set, $\phi(\boldsymbol{x},t)=0 \implies \boldsymbol{x}=(x,y,\eta(x,y,t))$. Moreover, the levelset function determines the unit vector normal to the interface ($\hat{\boldsymbol{n}}$), as well as the viscosity and density, via the relations $\mu(\phi)=\mu_B\left(1-H_\epsilon(\phi)\right)+\mu_T H_\epsilon(\phi)$ and $\rho(\phi)=\rho_B\left(1-H_\varepsilon(\phi)\right)+\rho_T H_\varepsilon(\phi)$ and respectively. The function $H_\epsilon(\phi)$ is a regularized Heaviside function, which is smooth across a width $\epsilon=1.5\Delta x$. Also, $\delta_\epsilon(s)=dH_\epsilon(s)/ds$ is a regularized delta function supported on an interval $[-\epsilon,\epsilon]$. Finally, Σ is the (constant) surface tension. These equations are solved using a projection method based on finite-volume discretization using a marker-and-cell grid. All other information about the algorithms used for the solution is given in Reference [45].

The reason for the inclusion of this extensive discussion of Equations (22) is because of the eery similarity of these equations to the diffusive-flux model (1). Thus, if instead of solving a levelset equation for ϕ we set $\mu(\phi)$ equal to the Krieger–Dougherty form, $\Sigma=0$,

and identify ϕ with the particle volume fraction and solve the diffusive-flux equation (3) for ϕ, we obtain a ready-made high-performance computing model capable of simulating transient suspensions in a channel flow. Such simulations could be performed relatively quickly leading to information about settling times of the particles, cuttings-bed formation, and pressure spikes following rapid start-up and shut-down of operations. This option is presented as an exciting avenue for future work.

Part II
Direct numerical simulation

In this section we survey the direct numerical simulation (DNS) possibilities for the problem at hand, our aim being to provide a robust basic method which can be extended to include all, or most, of the modelling requirements at hand.

IV. NUMERICAL APPROACHES

We consider the material of the pipe as having three main constituents; the drilling fluid, the drilling fluid with small particles of cuttings in suspension and larger particles of cuttings which break a continuum hypothesis. In addition to this complicated composition, the eccentricity and inclination of the pipe serve to break any symmetries requiring a DNS to model the annulus in its entirety. Also the boundary conditions of the inlet (and the inner wall if we hope to include rotation of the drill string) require careful consideration. We must be able to easily adjust the inflow of drilling fluid and cuttings in a consistent manner. Finally, in order to accurately solve any model equations it is likely some computational parallelism will be necessary given the large number of degrees of freedom which will be necessary.

Each consideration made above can be approached with a number of possible techniques. As a first step let us not consider the cuttings in suspension as a dispersed phase and assume there is a lower layer of settled sediment as a cuttings bed in the pipe. We can then consider the drilling fluid and cuttings as separate phases of non-Newtonian fluids of different density. Progress can thus be made on the fluid mechanical description via a multiphase approach. The literature abounds with possibilities for tackling multiphase flows numerically; a standard CFD (computational fluid dynamics) approach would be to employ a typical discretization of the equations for conservation of mass and momentum (using for example finite volume, finite element or finite difference method) with a volume of fluid approach to handle exchanges of momentum between the phases [13, 48] or a level-set method as in the TPLS method described in Section III. Another popular approach to multiphase problems is the smoothed particle hydrodynamic (SPH) method [20] which can handle complex geometries [1] (being a mesh free Lagrangian method). SPH solves evolution equations for discrete particles or parcels of fluid. Another "kinetic" type of approach is the so-called lattice Boltzmann method [4] which considers microscopic particles on a mesh or lattice evolved via the Boltzmann equation for collisions and advection. Both SPH and lattice Boltzmann have been used for multiphase and non-Newtonian flows to varying degrees [12, 21, 41, 42, 44].

As pointed out in Section III, any multiphase method employing some volume fraction approach (volume of fluid, or level-set) could be generalized to consider the dispersed phase. This gives some motivation to choosing a method of this type as a first step for the DNS.

The problem of coupled discrete particle-fluid models, to include the transport of the larger cuttings, is one which will require significant computational effort. Methods have been established to allow exchanges of momentum between classical fluid models and discrete Lagrangian particles [5, 7, 49]. These discrete particles must be accounted for individually, each being advected and having their contributions to the fluid momentum updated at every

timestep. This, as well as the additional variables associated with the multiphase approach, serves to steadily increase the number of degrees of freedom required at any given resolution. The development costs of such a complex algorithm are considerable.

Given the duration of this project, it was quickly decided that progress towards a numerical model would be achieved most effectively if use was made of existing open source packages in the field. This would reduce the time spent validating and debugging a new code hopefully resulting in a practical tool within a short time frame.

To this end we decided to investigate *OpenFOAM* for the fluid components of the method. OpenFOAM is an industry leading open source CFD toolbox and has rapidly developed to handle innumerable problems, not just in fluid mechanics but in solid mechanics, magnetohydrodynamics and electromagnetics. OpenFOAM is a mature suite of codes with established competency and offers an object-oriented programming approach giving us some confidence in its ability to satisfy a number of our needs and be extended in future work. Inded we found that, in time, OpenFOAM could cover almost all of the modelling requirements of the problem as described above (with help from some additional external libraries). OpenFOAM employs the finite volume method to solve momentum equations on arbitrary grids as such conserving mass exactly. Standard rheology models are included to model non-Newtonian flows, including the Hershel-Bulkley model (note due to the open source nature of OpenFOAM it is eminently possible, indeed encouraged by the OpenFOAM community, to introduce new features such as additional rheology models). Multiphase flows are handled by the volume of fluid approach, with an evolution equation for the volume fraction and a special limiter method for computing the advecting velocity [48]. OpenFOAM allows for almost any geometry and it is a simple enough task to create an eccentric annulus (see following sections) and inclination can be varied by projecting the gravity vector in the required direction.

A. InterFoam

In this section we briefly outline the components of OpenFOAM we make use of in the results to follow. We begin by setting up the solver for two-phase incompressible fluids and include the appropriate rheology for the two phases; drilling fluid and cuttings in suspension. The two-phase solver is known as *interFoam*. This is a DNS code; no turbulence modelling or parameterization is applied so care should be taken to ensure the simulation remains well resolved. Options for handling high Reynolds number flows (RANS, LES, etc.) can be found here[24]. As described above, interFoam employs a volume of fluid (VoF) approach to the two phase problem, evolving a scalar volume fraction via a sophisticated limiting algorithm (Multidimensional Universal Limiter with Explicit Solution; MULES) to accurately apply advecting velocities. As such the interface is never sharply defined but occupies the region where the phase fraction transitions from 0 to 1, typically a small number of cells wide (quantitative analysis should only be applied when this interface region is well resolved). The momentum equation is solved in a standard CFD manner, using a collocated finite-volume discretization (with Pressure Implicit with Splitting of Operators (PISO) method [46]) with the surface tension effects at the interface explicitly included. (Note, as a first attempt at modelling the flow at hand, we neglect the effect of surface tension at the liquid-liquid interface). For brevity a full mathematical description of the numerical method is avoided here, however extensive references exist for many of the individual components. A very good reference by Deshpande *et. al.* [6] provides quite a thorough description of interFoam itself,

a literature review its recent uses in research, and some validation of its performance and shortcomings, including some discussion of known numerical issues for numerical solution of multiphase flows. In particular emphasis is made on the importance of accurately resolving and capturing the interface, something that should be kept in mind when performing production runs of the model.

InterFoam (indeed any OpenFOAM solver) contains a vast array of options for timestepping, interpolation, linear solvers, tolerances, mesh orthogonality corrections and gradient schemes, too lengthy to list exhaustively here (see online documentation [28]). Suffice to say we retain the default choices; Euler timestepping, preconditioned conjugate-gradient solvers and linear interpolations for face centered values, except from the limiter (VanLeer) and fluxes (upwind). Future work could evaluate the performance of these choices.

1. Rheology Models

We have the ability with OpenFOAM to apply a number of rheology models for non-Newtonian fluids via an effective viscosity. The options available are Cross, power law, Bird-Carreau and Herschel-Bulkley. We employ the Herschel-Bulkley model with the parameters based on a type 3 drilling mud [14]. N.B. in OpenFoam the parameters are set in the *transportProperties* file (see [27]) and must be divided by density. We assume a density of $\rho_1 = 1027 kgm^{-3}$ for the drilling fluid, and $\rho_2 = 2191 kgm^3$ for the sediment layer.

2. Mesh generation and pipe geometry

OpenFOAM is primarily used in an industrial setting for a variety of fluid flow problems and as such is fully capable of tackling complex geometries. The discretization is quite general, allowing any polyhedral shaped control volumes in the mesh. This means that a number of mesh generation tools can be used and converted to the OpenFOAM format. In particular, for straightforward meshes, OpenFOAM comes with the *blockMesh* utility, allowing mesh geometries to be constructed via prescribed hexahedral blocks (whose edges can be straight or curved). It is a relatively straightforward exercise to create an annular pipe using blockMesh, providing care is taken to properly define the boundary patches. We create 4 blocks, each a 90° wedge of the annulus, offset by 45° from the vertical. It then becomes a rather messy procedure to include eccentricity by hand. Because of this, we have written a short FORTRAN program "meshgen" to generate the necessary *blockMeshDict* file (the dictionary file used by blockMesh to create the mesh). The FORTRAN program reads the pipe dimensions and eccentricities as its arguments, builds the dictionary file and once this is in place blockMesh can be run to generate the necessary mesh files.

Figure 7 shows a typical mesh for the eccentric annular pipe. Note OpenFoam always employs a Cartesian coordinate system so the mesh geometry must be specified as such. Also recall we incline the pipe by rotating the gravity vector (a simple exercise as gravity can be modified at runtime as one variable in the OpenFoam case, see Appendix B), therefore we define the y direction as the stream wise direction and the xz plane as pipe cross sections such that we incline the pipe ($\boldsymbol{g}$) in the zy plane; 0 inclination corresponds to a horizontal pipe and 90° to vertical. Eccentricity in the x and z directions can then both be specified as arguments in meshgen, along with the stream wise, radial and angular resolutions for each block.

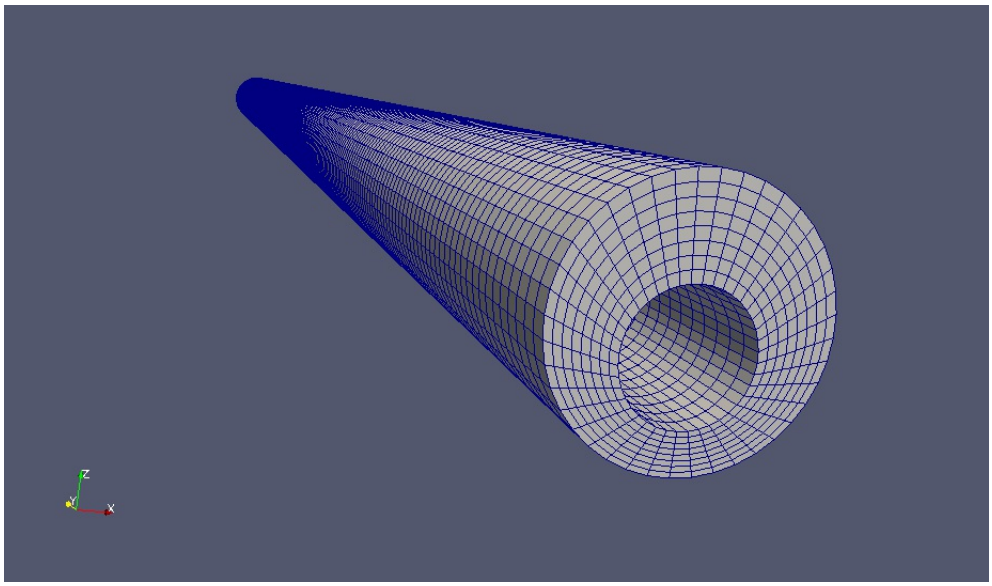

FIG. 7. Figure showing the mesh configuration for a typical annular pipe with 40% eccentricity and a total of 80000 cells.

In the results to follow we consider a concentric pipe length of 3 metres, outer diameter 0.125m and inner radius 0.06m to correspond to the thesis of Larsen [16]. We use 250 cells in the stream wise direction, 40 around the azimuthal angle and 8 in the radial direction giving a mesh of 80000 cells.

We will only consider a single mesh configuration per run, however OpenFOAM is capable of including adaptive mesh refinement or moving mesh strategies which may prove useful for high resolution simulations at a later date. For details of the mesh specification and blockMesh utility see documentation at [29].

3. Boundary and Initial Conditions

The application of boundary and initial conditions in the OpenFoam framework is applied in the "0" directory, where individual files are present for each variable (see appendix **??** on OpenFoam case structure). We make choices which are easy to implement and with the motivation that a long time simulation will lead to an appropriate steady state, rather than be physically relevant at the inlet.

We assume initially the fluid on the bulk in the annulus is only drilling fluid (no sediment phase) which is at rest. An inlet boundary condition on the bottom end ($y = 0$), outflow on the top ($y = 3m$) and a no-slip condition on the interior walls ($r = \sqrt{x^2 + z^2} = 0.03$ & 0.0625).

The inflow condition is moderately troublesome as we must carefully apply appropriate velocities on the drilling fluid phase and the sediment phase. By default boundary conditions are only easily set in OpenFoam by uniform value (or gradients) on mesh boundary patches (block faces). For this reason we must fix the interface between the phases and the inflow condition of each phase at a boundary patch edge. Therefore for these simulations the inflow of sediment occurs in the lower 90° wedge of the mesh, the idea being that far down the pipe the profile will settle into a steady state at a height which varies with the inflow velocity. We

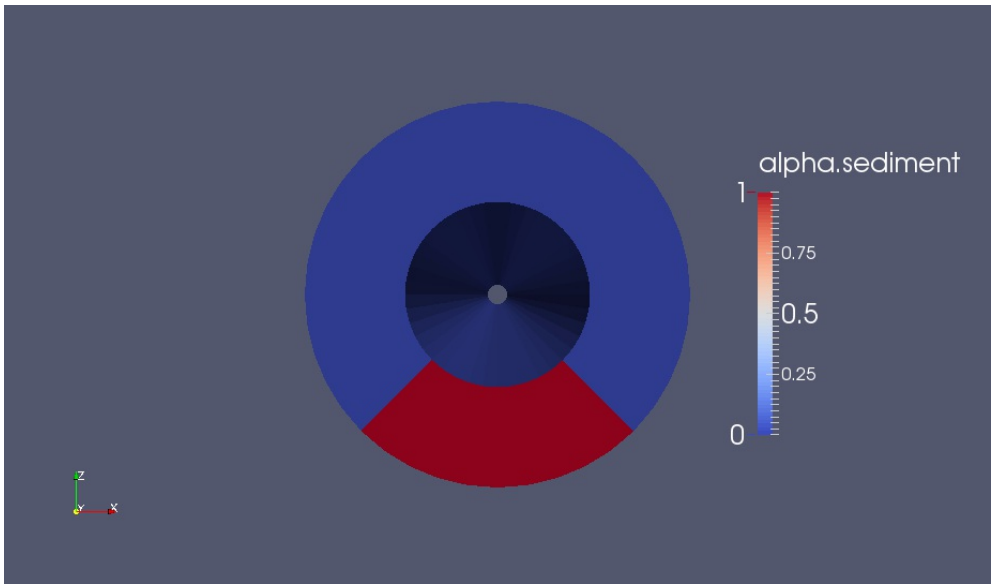

FIG. 8. Inlet of annulus showing the phase fraction boundary condition across the lower quarter boundary patch for the concentric case.

stress again that these simulations are to be considered as a starting point for developing the DNS into a quantitative predictive tool, rather than be immediately informative. We apply inflow velocities which are *roughly* comparable to the experimental values given in the thesis of Larsen [16]. Drilling fluid flow rate is always set to $1.55ms^{-1}$ and sediment flow rate is varied between 0.095 and $0.38ms^{-1}$.

An add-on exists for OpenFoam known as swak4Foam [30] which will allow more general boundary conditions and bulk initial data. Data can be set by an algebraic expression, for example based of the cell or face centre so that one is not restricted to uniform values on boundary patches. We provide an example for use with swak4Foam in the companion material.

4. Parallelism, post-processing and visualisation

While it is eminently possible to run the cases considered here as a serial, single processor job, OpenFoam is readily capable of parallel execution [31] and ships with the OpenMPI library. The case of interest is preprocessed and domain decomposed onto the specified number of processors (automatically using the *decomposePar* utility to distribute the work evenly). Output is then created per processor (as usual for MPI I/O) and the case can be reconstructed in post-processing (via *reconstructPar*). In the results to follow we run on the ICHEC machine Fionn [32] which is already set up with OpenFoam [33].
Each run of an OpenFoam solver produces a specially formatted output data, creating a directory of variables at each write interval. The method of visualisation for this data is using the *ParaView* open source visualisation software [34]. OpenFoam ships with a plugin for ParaView called *paraFoam* to set up the ParaView environment for each case.

B. Some results

We present some preliminary results from the execution of the interFoam program as described in the sections above. Please note these results really serve as a demonstration of the execution of an OpenFoam case *close* to the modelling requirements of this project; any quantitative study should be accompanied by a thorough validation and evaluation of all the algorithms in use.

We show three runs each with a different sediment inflow; (A) $u_{sed} = 0.095$, (B) $u_{sed} = 0.19$, (C) $u_{sed} = 0.38$. As described in the previous sections these cases are for a concentric annulus inclined at 30° to the horizontal. We run for $t = 60s$ and observe the propagation of the sediment layer up the annulus, all cases reach a steady state before the end of the simulation. As mentioned in the previous section, jobs are run in parallel across 24 cores each running for around 2 hours of CPU time. Movies are available here[35].

The principal difference between the cases, apart from the flow rate of the sediment phase, is the height of the eventual steady state which the sediment layer reaches. For the lowest flow rates the interface is below the annulus, and the larger flow rates the interface reaches higher up the walls. To observe the velocity profile across the interface we examine a probe line drawn in z at $x = 0.04625$ and $y = 15$ for the final time $t = 60s$. This line cuts the annular region at the midpoint (in x), chosen such that the interface will appear in all three cases (see Figure 10). These velocity profiles, together with a curve of phase fraction are shown in figure 9 and an end on view of the interface is shown in Figure 10. We also make note of the approximate time that the cuttings bed takes to reach the top of the pipe ($y = 3m$) for each three cases. Case (A) takes $20s$, (B) takes $23s$, (C) takes $15s$. At first glance these values may seem counter-intuitive: one would expect the faster the inflow velocity, the faster the propagation up the annulus. We notice that the intermediate velocity, case (B), $u_{sed} = 0.19ms^{-1}$ takes the longest. We conjecture this is due to the increased surface area of sediment phase in contact with the interior walls and the decreased interface in contact with the drilling fluid when the inflow is such that the sediment phase reaches the annular centre. The interior walls contribute more drag and the drilling fluid less entrainment. When the inflow velocity is $u_{sed} = 0.38ms^{-1}$ in case (C), the flow is now large enough to overcome the penalty of the annular geometry, relative to the low-inflow cases. Note, we do not consider the effect of the drilling fluid flow rate.

Figures 11–13 show the propagation of the sediment phase up the annular pipe, with snapshots at $t = 5s$, $15s$, and $60s$. These figures give some indication as to the speed at which the interface propagates up the pipe. Also note the interface is coloured with velocity magnitude, giving some indication of the internal velocity profile. At the outlet boundary ($y = 3m$) we see the fluids overtopping the edge, forming a (roughly) 30° angle in the yz-plane due to the inclination of the pipe. A further investigation of the effects of inclination and eccentricity are left for future work once the method is fully validated.

C. Future developments

Opportunities for developing the method and validating the numerics are extensive. It was discovered late in the course of the project that a less well documented OpenFoam solver exists called "settlingFoam" which models a particle suspension as a dispersed phase via a drift-flux model [3]. In the future it might be worth understanding this solver in detail and migrating the current set up from interFoam to settlingFoam to determine the effect of

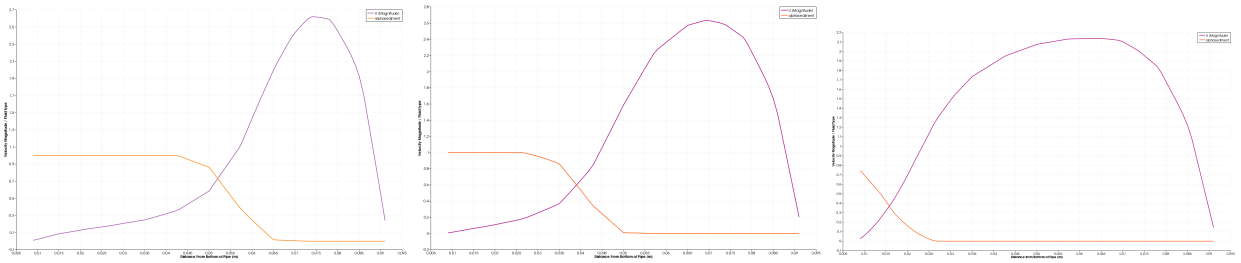

FIG. 9. In this figure we show velocity magnitudes (purple) and sediment volume fraction for a line in z drawn for constant $x = 0.04625m$ and $y = 15m$. The three figures are for three inflow (of sediment phase) values, from (A)-(C) left to right $u_{sed} = 0.095ms^{-1}$, $u_{sed} = 0.19ms^{-1}$ and $u_{sed} = 0.38ms^{-1}$.

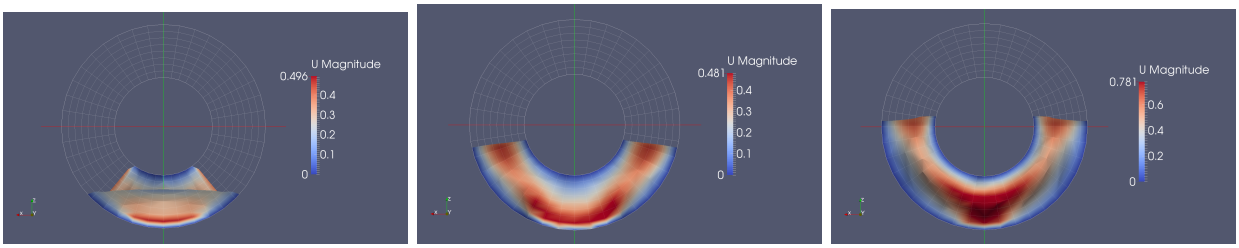

FIG. 10. In this figure we show the interface between the phases, coloured with velocity magnitude viewed directly down the pipe from $y = 3m$. The three figures are for three inflow (of sediment phase) values, from (A)-(C) left to right $u_{sed} = 0.095ms^{-1}$, $u_{sed} = 0.19ms^{-1}$ and $u_{sed} = 0.38ms^{-1}$. Notice the variation in the interface height for the 3 cases. Notice for (A), the lowest flow rate, we can see the length of the pipe to the inflow patch (see figure 8).

particle fluxes and compare to the results of the first part of this report.

We suggest the first step should be a thorough validation of the method. This could be achieved by some reduction of the complexity considered, for example a simplified channel geometry or considering a single phase, and comparison against some published results [2, 8, 39] or the TPLS solver.

As discussed in section IV A 3, we can apply more general boundary and initial conditions using the "groovyBC" and "funkySetFields" utilities in the swak4Foam add-on. This will also allow the application of inner pipe rotation by a no-slip angular velocity on the inner boundary of the annulus.

The final element of additional complexity we can suggest for the progression of the DNS is to include the effect of discrete larger cuttings via a coupling of the OpenFoam solver to a direct element method (DEM). While OpenFoam has some DEM functionality [36] there as yet appears to be no fluid-particle, particle-fluid coupling functionality. An open source method for the coupling of a DEM algorithm to the CFD of OpenFoam does exist however called "CFDEM" [25]. On their website they show several examples of modelling of coupled particles with several OpenFoam cases. It is our expectation that one could apply this method to the OpenFoam cases successfully, but some work will be required to understand

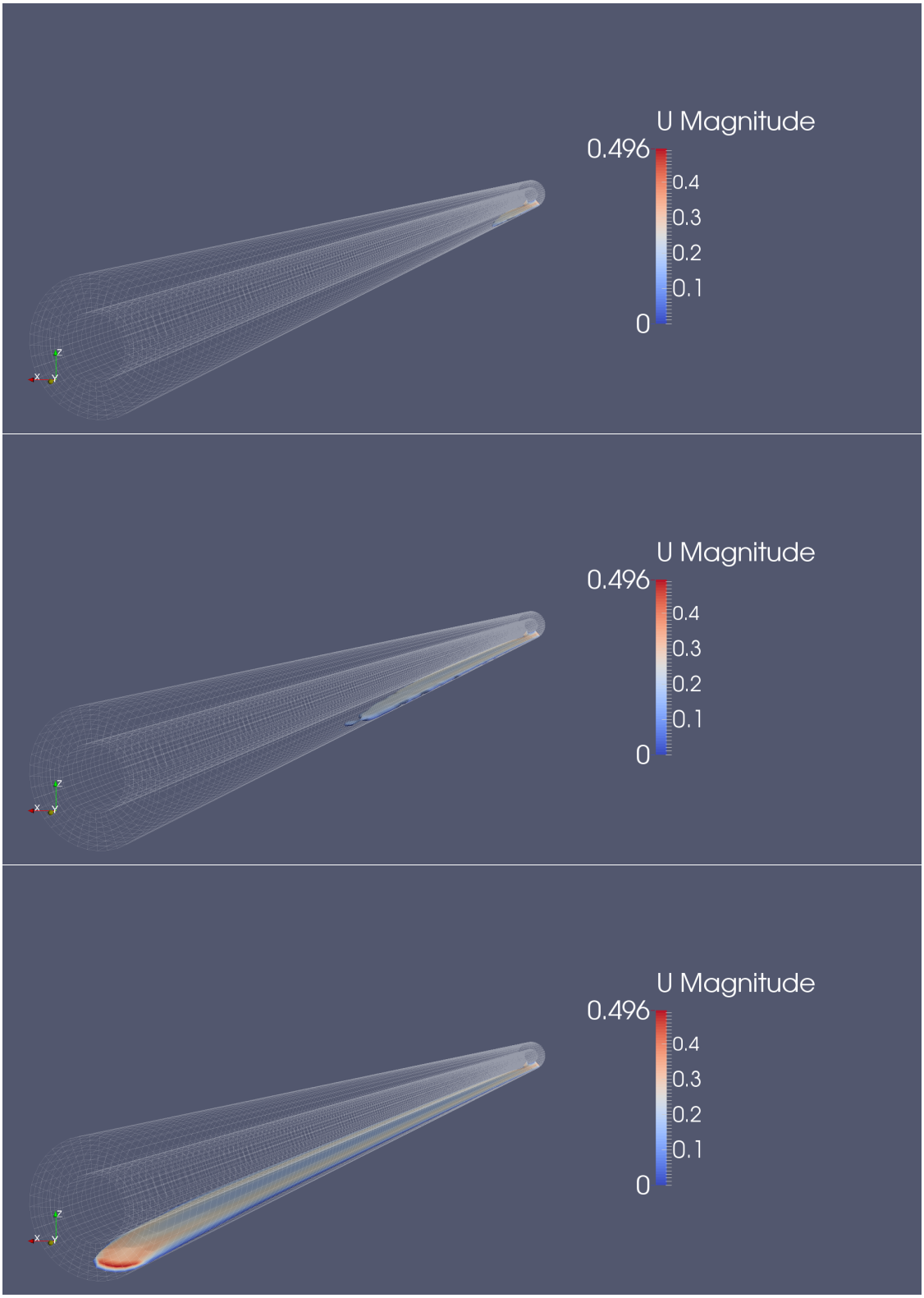

FIG. 11. In this figure we show the propagation of the sediment phase up the annulus for the case (A) $u_{sed} = 0.095ms^{-1}$ for times $t = 5s$, $15s$ and $60s$ from top to bottom, colours show velocity magnitude.

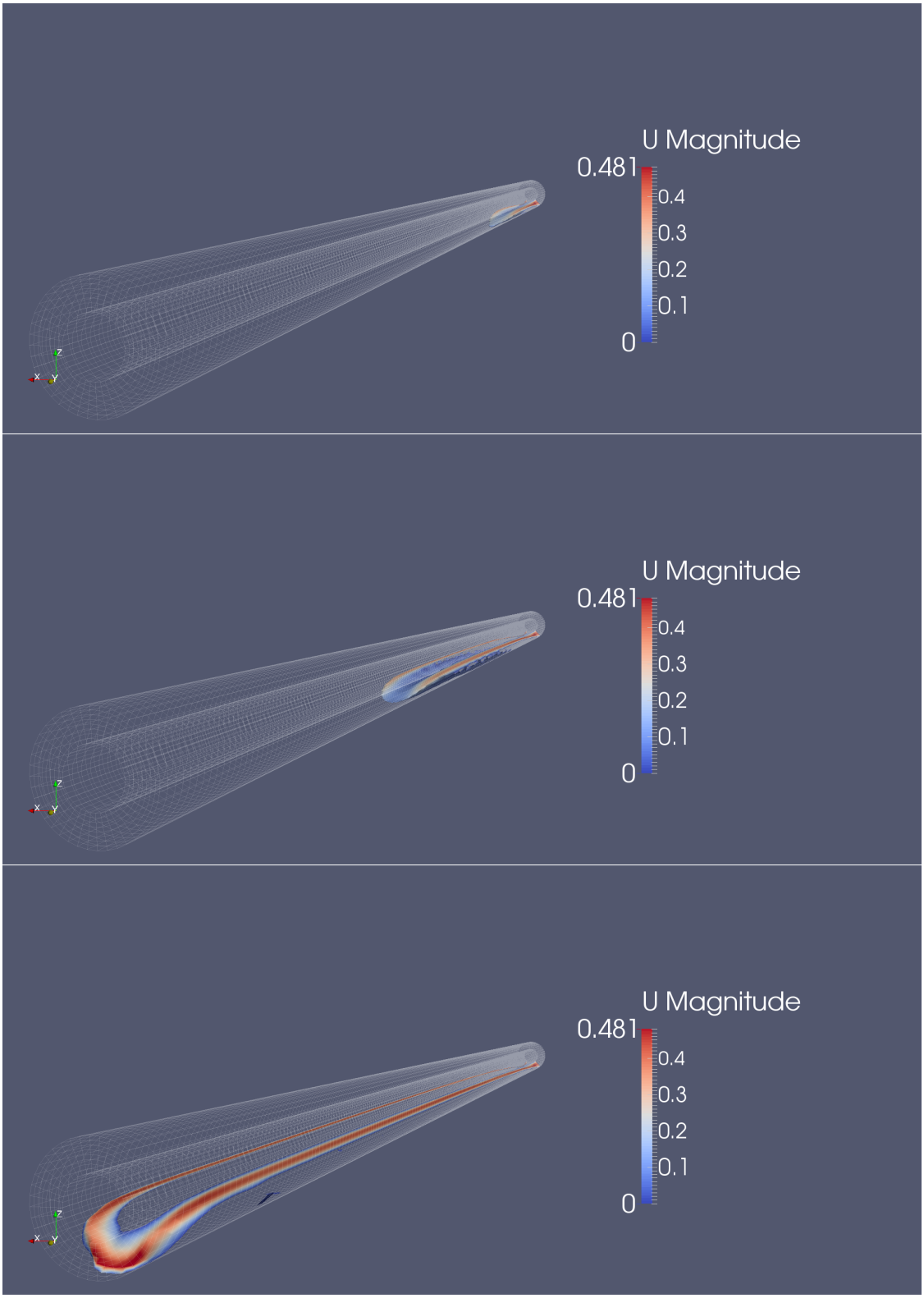

FIG. 12. In this figure we show the propagation of the sediment phase up the annulus for the case (B) for times $t = 5s$, $15s$ and $60s$ from top to bottom, colours show velocity magnitude.

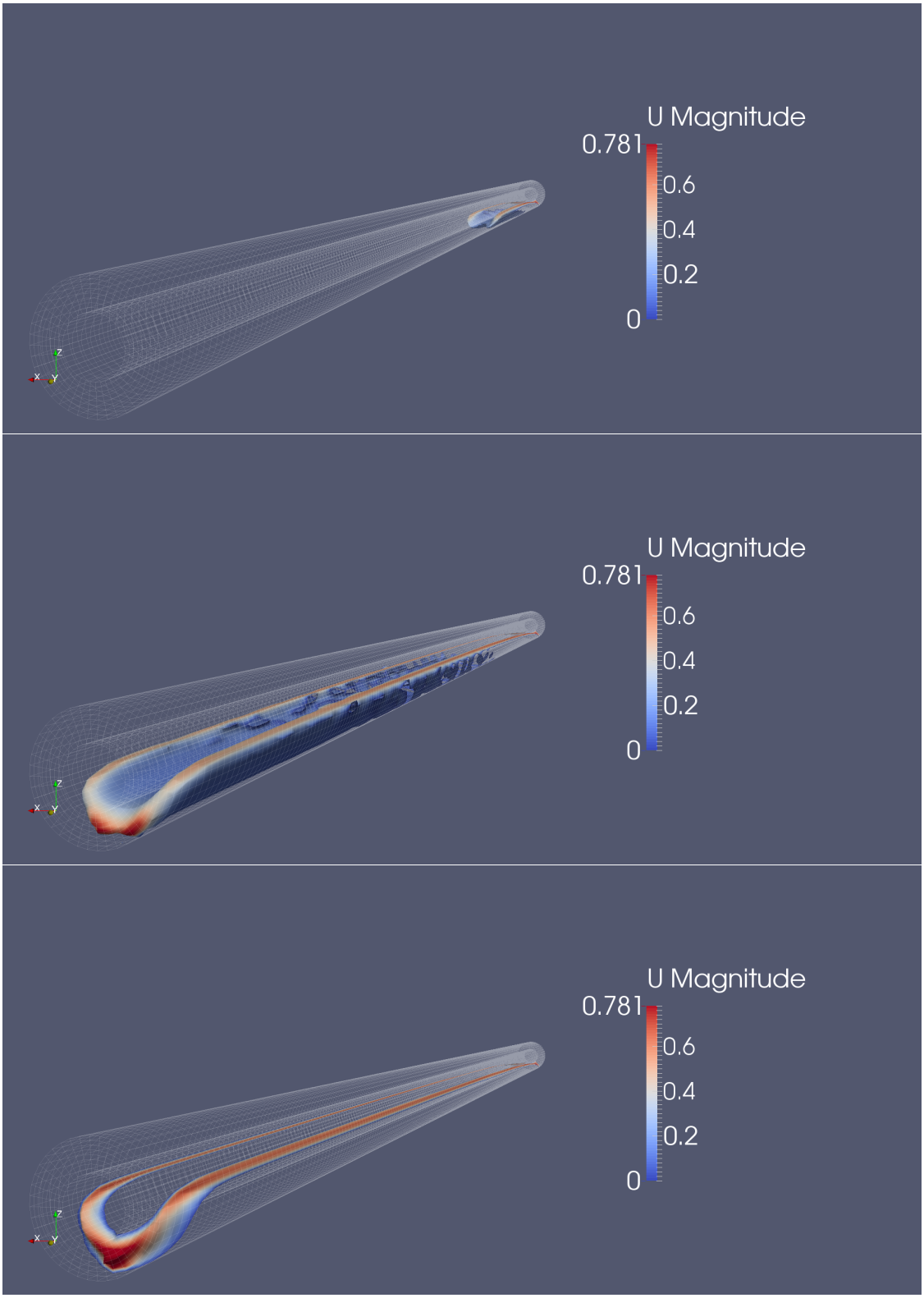

FIG. 13. In this figure we show the propagation of the sediment phase up the annulus for the case (C) for times $t = 5s$, $15s$ and $60s$ from top to bottom, colours show velocity magnitude.

the code, compile and correctly implement it alongside the existing solver. One would also expect such a model to be extremely computationally demanding and it is likely to require access to an HPC facility for serious computations.

V. CONCLUSIONS

Part 1

In this Report, we have formulated a model for the cuttings suspended in the drilling fluid based on a continuum hypothesis. A mixture momentum and mass balance is prescribed, as well as a diffusive-flux evolutionary equation for the cuttings volume fraction. The various fluxes in the volume-fraction equation are constituted using Phillips-type shear-induced diffusive migration. A one-dimensional fully-developed version of this equation is solved in channel, leading to expressions for the particle and mixture volumetric fluxes as a function of flow parameters, notably $(\mathrm{Re}\,\mathrm{Fr}^2, \Phi)$. In order to make comparisons with experiments (e.g. Reference [17]), it will be necessary to account for the non-Newtonian nature of the suspending drilling mud. The report outlines how this can be done, albeit that some work (possibly amounting to no more than a thorough literature review) is needed to constitute the viscosity and settling function as a function of volume fraction, in the non-Newtonian regime.

Crucially, it is outlined how an existing high-performance flow solver can be modified to take account of suspension dynamics. This would provide a way of understanding the transient suspension dynamics in a timely fashion, without necessarily needing to resort to full direct numerical simulation.

Some cautionary words are appropriate here. While the model of Phillips *et al.* [40] is well known to produce satisfactory results for unidirectional flows [37], for two- and three-dimensional dynamical flows, the full suspension balance model of Nott and Brady [37] may be required. Also, there are more recent developments concerning the constitutive modelling of some stress terms (including the bulk viscosity, see Reference [38]).

For these reasons, direct numerical simulation is important. This approach will also shed light on the effects of complex geometry on the problem, and the effect of the rotation of the inner tube on the hydrodynamics and suspension dynamics. The same approach can be used (this time in an idealized geometry) to investigate and determine the correct bulk constitutive relations needed to close the diffusive-flux models (or other continuum models) for the case wherein the suspending fluid has a non-Newtonian rheology. Thus, direct numerical simulations were also investigated as part of this project.

Part 2

The second part of this report has presented a potential approach for a direct numerical simulation framework for the problem at hand. A first attempt at some simulation is presented using the OpenFOAM CFD codes and a two phase model for each of the drilling fluid and a settled sediment layer, or cuttings bed. This is achieved numerically using a finite-volume discretisation of the transport equations with a volume of fluid treatment of the phase fraction. The complexity of OpenFOAM is extensive and allows us to tackle a large number of the modelling requirements at hand. In particular we have shown the ease

of setting up the eccentric, inclined annular geometry of the problem. We also satisfy the non Newtonian rheology of the flow. The initial runs show the possible power of the method; already we show some of the physics of the problem when varying just one free parameter.

As presented the open problem of cuttings transport in an eccentric, inclined annular pipe with non Newtonian drilling fluid and inner cylinder rotation contains a great many free parameters. It is our hope that the method and modelling strategy presented allows the opportunity to investigate many of these. In particular it is now a trivial exercise to vary the pipe eccentricity, inclination, inflow rates and fluid properties. We have provided some suggestion as to where the method can be extended to include some of the features we do not have time to include; namely inner cylinder rotation, dispersed phase and discrete particles. In due course it is believed the direct numerical simulation is achievable with the methods presented here.

Appendix A: Derivation of equation for particle-averaged shear stress

Consider a particle located at $\boldsymbol{x}_0$ in the domain. The mixture shear stress at this point is $\sigma(\boldsymbol{x}_0)$. Instead of using this quantity in the diffusive-flux model, we consider instead the following averaged shear stress, where the average is taken in the L^2 norm:

$$\hat{\sigma}(\boldsymbol{x}_0) = \left[\frac{1}{|S(\boldsymbol{x}_0,\mathcal{R})|}\int_{S(\boldsymbol{x}_0,\mathcal{R})}\sigma^2(\boldsymbol{x})\mathrm{d}S\right]^{1/2} \tag{A1}$$

where $S(\boldsymbol{x}_0,\mathcal{R})$ is the sphere of centre $\boldsymbol{x}_0$ and radius $\mathcal{R}$ and $|S(\boldsymbol{x}_0,\mathcal{R})|$ is the surface area of the sphere (i.e. particle surface area, equal to $2\pi\mathcal{R}$ in two dimensions, and $4\pi\mathcal{R}^2$ in three dimensions.) Here, the L^2 norm is chosen because it renders the following calculations – in particular, integrals – straightforward. Also, $\mathrm{d}S$ denotes an infinitesimal patch of area on the boundary sphere $S(\boldsymbol{x}_0,\mathcal{R})$.

Because the particles are assumed to have a small radius in comparison to the channel height, the shear stress is expanded in a Taylor expansion, centred at the particle centre, to first order:

$$\sigma(\boldsymbol{x}) = \sigma(\boldsymbol{x}_0) + (\boldsymbol{x}-\boldsymbol{x}_0)\cdot\nabla\sigma\big|_{\boldsymbol{x}_0}. \tag{A2}$$

We denote the radicand in Equation (A1) by $\mathcal{I}$; we have

$$\begin{aligned}
\mathcal{I} &= \frac{1}{|S(\boldsymbol{x}_0,\mathcal{R})|}\int_{S(\boldsymbol{x}_0,\mathcal{R})}\sigma^2(\boldsymbol{x})\mathrm{d}S,\\
&= \frac{1}{|S(\boldsymbol{x}_0,\mathcal{R})|}\int_{S(\boldsymbol{x}_0,\mathcal{R})}\left[\sigma(\boldsymbol{x}_0)+(\boldsymbol{x}-\boldsymbol{x}_0)\cdot\nabla\sigma\big|_{\boldsymbol{x}_0}\right]^2\mathrm{d}S,\\
&= [\sigma(\boldsymbol{x}_0)]^2 + 2|S(\boldsymbol{x}_0,\mathcal{R})|^{-1}\sigma(\boldsymbol{x}_0)\left(\nabla\sigma\right)_{\boldsymbol{x}_0}\cdot\int_{S(\boldsymbol{x}_0,\mathcal{R})}(\boldsymbol{x}-\boldsymbol{x}_0)\,\mathrm{d}S\\
&\qquad + |S(\boldsymbol{x}_0,\mathcal{R})|^{-1}\int_{S(\boldsymbol{x}_0,\mathcal{R})}[(\boldsymbol{x}-\boldsymbol{x}_0)\cdot\nabla\sigma\big|_{\boldsymbol{x}_0}]^2\,\mathrm{d}S,\\
&= [\sigma(\boldsymbol{x}_0)]^2 + \tfrac{1}{2}\mathcal{R}^2\left(\nabla\sigma\big|_{\boldsymbol{x}_0}\right)^2,
\end{aligned}$$

hence

$$\hat{\sigma}(\boldsymbol{x}_0) = \sqrt{[\sigma(\boldsymbol{x}_0)]^2 + \epsilon^2\left(\nabla\sigma\big|_{\boldsymbol{x}_0}\right)^2}, \qquad \epsilon = \mathcal{R}/\sqrt{2}, \tag{A3}$$

valid to first order in a Taylor expansion.

To understand how Equation (A3) is worked into a balance model for the shear stress and the volume fraction profiles, we start with Equation (11) in the main text, viz.

$$D_\mathrm{c}\phi\frac{\mathrm{d}}{\mathrm{d}\tilde{z}}\left(\frac{\sigma}{\mu}\phi\right) + D_\mathrm{v}\phi\frac{\sigma}{\mu^2}\frac{\mathrm{d}\mu}{\mathrm{d}z} + \frac{2(r-1)\phi(1-\phi)}{9\mu(\phi)}\mathrm{Re}\,\mathrm{Fr}^2\cos\alpha\,\omega(z) = 0.$$

Next, all instances of σ are replaced with $\hat{\sigma}$, to yield

$$D_\mathrm{c}\phi\frac{\mathrm{d}}{\mathrm{d}\tilde{z}}\left(\frac{\hat{\sigma}}{\mu}\phi\right) + D_\mathrm{v}\phi\frac{\hat{\sigma}}{\mu^2}\frac{\mathrm{d}\mu}{\mathrm{d}z} + \frac{2(r-1)\phi(1-\phi)}{9\mu(\phi)}\mathrm{Re}\,\mathrm{Fr}^2\cos\alpha\,\omega(z) = 0. \tag{A4}$$

Using the Krieger–Dougherty relation $\mu = [1-(\phi/\phi_{\rm m})]^{-2}$, the μ-derivatives are computed and Equation (A4) reduces to

$$\left[1+\frac{2(D_{\rm v}-D_{\rm c})}{D_{\rm c}}\frac{\phi}{\phi_{\rm m}-\phi}\right]\hat{\sigma}\frac{{\rm d}\phi}{{\rm d}z} = -\frac{{\rm d}\hat{\sigma}}{{\rm d}z}\phi + \tfrac{2}{9D_{\rm c}}{\rm Re}\,{\rm Fr}^2(r-1)\cos\alpha(1-\phi)\omega(z). \qquad \text{(A5)}$$

The following identities will now be used to compute ${\rm d}\hat{\sigma}/{\rm d}z$:

$$\begin{aligned}\hat{\sigma} &= \sqrt{\sigma^2+\epsilon^2\left(\frac{{\rm d}\sigma}{{\rm d}z}\right)^2},\\ \frac{{\rm d}\sigma}{{\rm d}z} &= -1+{\rm Re}\,{\rm Fr}^2\sin\alpha\rho(\phi),\\ \frac{{\rm d}^2\sigma}{{\rm d}z^2} &= {\rm Re}\,{\rm Fr}^2\sin\alpha(r-1)\frac{{\rm d}\phi}{{\rm d}z}.\end{aligned}$$

Thus,

$$\begin{aligned}\frac{{\rm d}\hat{\sigma}}{{\rm d}z} &= \frac{1}{\hat{\sigma}}\left(\sigma\frac{{\rm d}\sigma}{{\rm d}z}+\epsilon^2\frac{{\rm d}\sigma}{{\rm d}z}\frac{{\rm d}^2\sigma}{{\rm d}z^2}\right),\\ &= \frac{\sigma}{\hat{\sigma}}\frac{{\rm d}\sigma}{{\rm d}z}+\frac{\epsilon^2}{\hat{\sigma}}\frac{{\rm d}\sigma}{{\rm d}z}\frac{{\rm d}^2\sigma}{{\rm d}z^2},\\ &= \frac{\sigma}{\hat{\sigma}}\frac{{\rm d}\sigma}{{\rm d}z}+\frac{\epsilon^2}{\hat{\sigma}}\left[{\rm Re}\,{\rm Fr}^2\sin\alpha(r-1)\frac{{\rm d}\phi}{{\rm d}z}\right].\end{aligned}$$

This last equation is now substituted into Equation (A5):

$$\left[1+\frac{2(D_{\rm v}-D_{\rm c})}{D_{\rm c}}\frac{\phi}{\phi_{\rm m}-\phi}\right]\hat{\sigma}\frac{{\rm d}\phi}{{\rm d}z} = -\left\{\frac{\sigma}{\hat{\sigma}}\frac{{\rm d}\sigma}{{\rm d}z}+\frac{\epsilon^2}{\hat{\sigma}}\left[{\rm Re}\,{\rm Fr}^2\sin\alpha(r-1)\frac{{\rm d}\phi}{{\rm d}z}\right]\right\} + \tfrac{2}{9D_{\rm c}}{\rm Re}\,{\rm Fr}^2(r-1)\cos\alpha(1-\phi)\omega(z).$$

Re-arrange:

$$\left[1+\frac{2(D_{\rm v}-D_{\rm c})}{D_{\rm c}}\frac{\phi}{\phi_{\rm m}-\phi}+\frac{\epsilon^2}{\hat{\sigma}^2}{\rm Re}\,{\rm Fr}^2\sin\alpha(r-1)\right]\hat{\sigma}\frac{{\rm d}\phi}{{\rm d}z} = -\frac{\sigma}{\hat{\sigma}}\frac{{\rm d}\sigma}{{\rm d}z}+\tfrac{2}{9D_{\rm c}}{\rm Re}\,{\rm Fr}^2(r-1)\cos\alpha(1-\phi)\omega(z),$$

hence

$$\frac{{\rm d}\phi}{{\rm d}z} = \frac{-\frac{\sigma}{\hat{\sigma}}\frac{{\rm d}\sigma}{{\rm d}z}+\frac{2}{9D_{\rm c}}{\rm Re}\,{\rm Fr}^2(r-1)\cos\alpha(1-\phi)\omega(z)}{\left[1+\frac{2(D_{\rm v}-D_{\rm c})}{D_{\rm c}}\frac{\phi}{\phi_{\rm m}-\phi}+\frac{\epsilon^2}{\hat{\sigma}^2}{\rm Re}\,{\rm Fr}^2\sin\alpha(r-1)\right]\hat{\sigma}},$$

which is Equation (14) in the main text.

Appendix B: Installing and using OpenFOAM

In this appendix we provide some brief comments on installing and using OpenFOAM.

OpenFOAM can be built on a number of platforms but is easiest compiled on a Linux system. A large number of HPC systems will already have OpenFOAM installed (e.g. ICHEC in Ireland). Full documentation and instructions on the installation and use of the codes can be found online at[26]. In short all of the results we show here are created using standard solvers built at installation and following a familiar pattern at runtime. The documentation shows how to set up a case[27] and several tutorials are provided to familiarise the user with the behaviour of the code. We recommend running some simple relevant tutorial cases to get used to the format of OpenFOAM and ensure that the configuration you have is working correctly. Attached (and provided here[28]) are the case files for setting up the mesh and runs in serial and parallel, along with a README to provide practical instructions. Note for ease of use, and to ensure the correct sequence of set-up steps, we have written some bash scripts to automate some of the set-up, called *Allrun, Allmesh* and *Allclean*. These will hopefully be clear given the README and the online OpenFOAM documentation.The OpenFOAM website also describes how to install ParaView and set up the plugins to read OpenFOAM cases.

Changing parameters of the problem will either be handled in the preprocessing (e.g. problem geometry in meshgen/Allmesh) or in the individual case files (e.g. "0/U" for boundary conditions, "constant/transportProperties" for rheology, "constant/g" for inclination etc.)

Note the swak4Foam library requires downloading and compiling separately *after* OpenFOAM is installed on your system [32].

[1] Carla Antoci, Mario Gallati, and Stefano Sibilla. Numerical simulation of fluid–structure interaction by SPH. *Computers & Structures*, 85(11-14):879–890, June 2007.

[2] S H Bittleston, J Ferguson, and I A FRIGAARD. Mud removal and cement placement during primary cementing of an oil well – Laminar non-Newtonian displacements in an eccentric annular Hele-Shaw cell. *Journal of Engineering Mathematics*, 43(2-4):229–253, August 2002.

[3] D Brennan. The numerical simulation of two phase flows in settling tanks, 2001.

[4] S Chen and G D Doolen. Lattice Boltzmann method for fluid flows. *Annual Review of Fluid Mechanics*, 30(1):329–364, 1998.

[5] C N Davies. Particle-fluid interaction. *Journal of Aerosol Science*, 10(5):477–513, 1979.

[6] Suraj S Deshpande, Lakshman Anumolu, and Mario F Trujillo. Evaluating the performance of the two-phase flow solver interFoam. *Computational Science & Discovery*, 5(1):014016, January 2012.

[7] J K Dukowicz. A particle-fluid numerical model for liquid sprays. *Journal of Computational Physics*, 35(2):229–253, 1980.

[8] M P Escudier, P J Oliveira, and F T Pinho. Fully developed laminar flow of purely viscous non-Newtonian liquids through annuli, including the effects of eccentricity and inner-cylinder rotation. *Journal of Heat and Fluid Flow*, 23(1):52–73, 2002.

[9] Zhiwu Fang, Andrea A Mammoli, John F Brady, Marc S Ingber, Lisa A Mondy, and Alan L Graham. Flow-aligned tensor models for suspension flows. *International journal of multiphase flow*, 28(1):137–166, 2002.

[10] Xavier Grandchamp, Gwennou Coupier, Aparna Srivastav, Christophe Minetti, and Thomas Podgorski. Lift and down-gradient shear-induced diffusion in red blood cell suspensions. *Physical review letters*, 110(10):108101, 2013.

[11] John Happel and Howard Brenner. *Low Reynolds number hydrodynamics: with special applications to particulate media*, volume 1. Springer, 1983.

[12] X He, S Chen, and R Zhang. A lattice Boltzmann scheme for incompressible multiphase flow and its application in simulation of Rayleigh–Taylor instability. *Journal of Computational Physics*, 152(2):642–663, 1999.

[13] C. W. Hirt and B. D. Nichols. Volume of fluid /VOF/ method for the dynamics of free boundaries. *Journal of Computational Physics*, 39:201–225, January 1981. doi:10.1016/0021-9991(81)90145-5.

[14] James Klotz and William Brigham. To Determine Herschel-Bulkley Coefficients. *Journal of Petroleum Technology*, 50(11), 1998.

[15] NJ. A. Klotz and W. E. Brigham. To determine the herschel-bulkley coefficients. *Journal of Petroleum Technology*, 50(11):80–81, 1998.

[16] Thor Inge F. Larsen. *A study of the critical fluid velocity in cuttings transport for inclined wellbores*. The University of Tulsa Graduate School, MSc Thesis, 1990.

[17] Thor Inge F. Larsen. *A Study of the Critical Fluid Velocity in Cuttings Transport for Inclined Wellbores*. PhD thesis, University of Tulsa, 1990.

[18] David Leighton and Andreas Acrivos. The shear-induced migration of particles in concentrated suspensions. *Journal of Fluid Mechanics*, 181:415–439, 1987.

[19] MK Lyon and LG Leal. An experimental study of the motion of concentrated suspensions in two-dimensional channel flow. part 1. monodisperse systems. *Journal of Fluid Mechanics*,

363:25–56, 1998.

[20] J Monaghan. Smoothed particle hydrodynamics. *Annual review of astronomy and astrophysics*, 1992.

[21] J J Monaghan and A Kocharyan. SPH simulation of multi-phase flow. *Computer Physics Communications*, 87(1-2):225–235, 1995.

[22] JF Morris and JF Brady. Pressure-driven flow of a suspension: Buoyancy effects. *International journal of multiphase flow*, 24(1):105–130, 1998.

[23] N Murisic, J Ho, V Hu, P Latterman, T Koch, K Lin, M Mata, and AL Bertozzi. Particle-laden viscous thin-film flows on an incline: Experiments compared with a theory based on shear-induced migration and particle settling. *Physica D: Nonlinear Phenomena*, 240(20): 1661–1673, 2011.

[24] Note1. `http://openfoam.org/features/turbulence.php`.

[25] Note10. `http://www.cfdem.com/`.

[26] Note11. `http://www.openfoam.org/`.

[27] Note12. `http://www.openfoam.org/docs/user/cases.php`.

[28] Note13. `http://mathsci.ucd.ie/~dan/irisCase.zip`.

[29] Note2. `http://www.openfoam.org/docs/user/mesh.php`.

[30] Note3. `http://openfoamwiki.net/index.php/Contrib/swak4Foam`.

[31] Note4. `http://www.openfoam.org/features/parallel-computing.php`.

[32] Note5. `https://www.ichec.ie/infrastructure/fionn`.

[33] Note6. `https://www.ichec.ie/infrastructure/software/OpenFOAM`.

[34] Note7. `http://www.paraview.org/`.

[35] Note8. `http://mathsci.ucd.ie/~dan/ESGI2014.html`.

[36] Note9. `http://www.openfoam.org/version2.0.0/lagrangian.php`.

[37] Prabhu R Nott and John F Brady. Pressure-driven flow of suspensions: simulation and theory. *Journal of Fluid Mechanics*, 275(1):157–199, 1994.

[38] M. Pavilis. The dependence of suspension viscosity on particle size, shear rate, and solvent viscosity, 2011.

[39] S PELIPENKO and I A FRIGAARD. Visco-plastic fluid displacements in near-vertical narrow eccentric annuli: prediction of travelling-wave solutions and interfacial instability. *Journal of Fluid Mechanics*, 520:343–377, 1999.

[40] Ronald J Phillips, Robert C Armstrong, Robert A Brown, Alan L Graham, and James R Abbott. A constitutive equation for concentrated suspensions that accounts for shear-induced particle migration. *Physics of Fluids A: Fluid Dynamics (1989-1993)*, 4(1):30–40, 1992.

[41] T N Phillips and G W Roberts. Lattice Boltzmann models for non-Newtonian flows. *IMA journal of applied mathematics*, 76(5):790–816, September 2011.

[42] Benedict W Ritchie and Peter A Thomas. Multiphase smoothed-particle hydrodynamics. *Monthly Notices of the Royal Astronomical Society*, 323(3):743–756, May 2001.

[43] Uwe Schaflinger. Transport of a sediment layer due to a laminar, stratified flow. *Fluid dynamics research*, 12(2):95, 1993.

[44] Songdong Shao and Edmond Y M Lo. Incompressible SPH method for simulating Newtonian and non-Newtonian flows with a free surface. *Advances in Water Resources*, 26(7):787–800, July 2003.

[45] L. Ó Náraigh, P. Valluri, D. M. Scott, I. Bethune, and P. D. M. Spelt. Linear instability, nonlinear instability and ligament dynamics in three-dimensional laminer two-layer liquid-liquid flows. *J. Fluid Mech.*, 750:464–506, 2014.

[46] Henk Kaarle Versteeg and Weeratunge Malalasekera. *An introduction to computational fluid dynamics*. the finite volume method. Prentice Hall, January 2007.

[47] HM Vollebregt, RGM Van Der Sman, and RM Boom. Suspension flow modelling in particle migration and microfiltration. *Soft Matter*, 6(24):6052–6064, 2010.

[48] Kent E Wardle and Henry G Weller. Hybrid Multiphase CFD Solver for Coupled Dispersed/Segregated Flows in Liquid-Liquid Extraction. *International Journal of Chemical Engineering*, 2013:1–13, 2013.

[49] B H Xu and Yu, AB. Numerical simulation of the gas-solid flow in a fluidized bed by combining discrete particle method with computational fluid dynamics. *Chemical Engineering Science*, 52(16):2785–2809, August 1997.

[50] Yiguang Yan and Joel Koplik. Transport and sedimentation of suspended particles in inertial pressure-driven flow. *Physics of Fluids (1994-present)*, 21(1):013301, 2009.